Engineering Structures 195 (2019) 223–230

Contents lists available at ScienceDirect

Engineering Structures

journal homepage: www.elsevier.com/locate/engstruct

Axial behavior of reinforced PP-ECC column and hybrid NSC-ECC column under compression

Fuhai Li[a,c], Zhihua Feng[a], Kailai Deng[b,c,*], Yongjiang Yu[a], Zhiming Hu[a], Hesong Jin[a]

[a] Department of Building Material, Southwest Jiaotong University, Chengdu 610031, China
[b] Department of Bridge Engineering, Southwest Jiaotong University, Chengdu 610031, China
[c] Key Laboratory of High-Speed Railway Engineering, Ministry of Education, Southwest Jiaotong University, Chengdu 610031, China

ARTICLE INFO

Keywords:
PP-ECC
Compressive behavior
Hybrid configuration
Volumetric stirrup ratio
Self-confining effect

ABSTRACT

Polypropylene engineered cementitious composites (PP-ECC) exhibit superior strength and strain hardening under tensile deformation, which is expected to enhance the anti-cracking performance and self-confinement of the plastic hinge region in structural columns. However, there is still a lack of fundamental studies on the compressive behavior of a reinforcement-confined PP-ECC column. This paper presents a proof-of-concept experimental study on the confined PP-ECC column and hybrid normal strength concrete (NSC)-ECC column. Two sets of reinforcement-confined columns were designed: a pure PP-ECC column and a hybrid C30-PP-ECC column. Then, static compression tests were carried out to prove the effectiveness of the confinement in enhancing the peak strength of the hybrid column with respect to pure PP-ECC columns. However, the deformability improvement was not remarkable, with an increase of only 3.2% from samples containing no stirrups to those containing stirrups at a volumetric ratio of 1.6%. An equation was proposed to predict the peak strength of the confined PP-ECC columns. This equation considered the contribution from the tensile capacity of PP-ECC to the circumferential confining effect of the columns. The hybrid column delivered better deformability but smaller peak strength compared with the pure PP-ECC columns. Some mechanical features of the hybrid column were discussed.

1. Introduction

In recent years, the engineered cementitious composite (ECC) has demonstrated evident advantages for crack resistance and tensile strain hardening [1–4]. Currently, polyvinyl alcohol (PVA) and polyethylene (PE) fibers are commonly used in ECCs. With the application of PVA and PE fibers, the tensile stress and ultimate deformability of an ECC can be larger than 3 MPa and 5%, respectively [5,6]. On the basis of advances with this material, many composite components or structures were developed and investigated to improve the structural deformability and crack resistance [7–9]. Choi et al. [10] reviewed the mechanical properties of ECC and its application in different structural components, such as beam-wall connections, coupling beams in walls, shear walls, and columns. Due to the excellent strain hardening behavior and ductility of ECC materials, these composite structures exhibited better deformability and energy dissipation capacity when used as reinforced ECC columns and ECC beam-column connections. The specimen failed after the ECC was crushed but only at very large deformation. However, the high cost of PVA and PE fibers hinder the large-scale promotion of ECC in practical engineering.

To reduce the cost, some hybrid structures were developed, which were composed of ECC material and traditional reinforced concrete (RC) materials. Maalej & Leong [11] employing the ECC material in the tensile area of the beam, and attached a fiber-reinforced polymer (FRP) sheet to the surface of the ECC material. The test results proved that using ECC material in the tension area can enhance the cohesive strength between the FRP sheet and ECC material and delay the debonding failure of the FRP sheet. Moreover, Maalej et al. [12] introduced the ECC material into the retrofit of masonry walls. The ECC layer was adopted to strengthen the out-of-plane resistance of masonry bricks. According to the quasi-static test, significant improvements in the load-carrying capacity and the ductility can be obtained by introducing the ECC layer. Finally, penetration failure occurred under a large concentrated load. Moreover, the ECC material can be used in combination with shape memory alloys to provide self-centering and crack resistance of pier columns [13,14]. Test results proved the effectiveness of the ECC material in limiting cracking. The crushing of ECC material occurred at the column base. Gencturk & Elnashai [15]

* Corresponding author at: Department of Bridge Engineering, Southwest Jiaotong University, Chengdu 610031, China.
E-mail address: kailai_deng@163.com (K. Deng).

https://doi.org/10.1016/j.engstruct.2019.06.010
Received 23 November 2018; Received in revised form 5 June 2019; Accepted 5 June 2019

Nomenclature

A_{cov}	area of cover layer
A_s	area of longitudinal reinforcement
C30	concrete with cube compressive strength of 30 MPa
E_c	elastic modulus of C30 concrete or ECC material
E_{c_ECC}	elastic modulus of ECC material
E_s	elastic modulus of rebar
F	overall axial load
F_{cov}	axial load of cover layer
F_s	axial load of longitudinal reinforcement
d	diameter
d_c	diameter of stirrup centerline
f_{co}	axial compressive strength of ECC material/C30 concrete
f_{ti}	initial cracking stress
f_{tu}	ultimate tensile stress
f_y	yielding strength of rebar
h	height
ε	axial compressive strain
$\varepsilon_{c\text{ - }C30}$	strain of C30 core at peak strength
$\varepsilon_{c\text{ - }ECC}$	strain of external PP-ECC layer at peak strength
$\varepsilon_{c\text{ - }H}$	strain under actual peak stress
ε_{co}	strain at peak compressive stress of ECC material/C30 concrete
ε_{tu}	ultimate tensile strain
ε_y	strain of reinforced steel at yield
σ_c	core concrete stress
σ_{CO}	concrete stress
σ_{CC}	fiber-reinforced concrete stress
σ_t	tensile stress of PP-ECC
σ_l	circumferential confining stress
ρ	sectional reinforcement ratio
ρ_v	volumetric stirrup ratio
μ	Poisson's ratio

proposed a cyclic constitutive model for the ECC component under cyclic load, which reliably predicts the hysteretic behavior of the ECC component. On the basis of this model, a hybrid simulation was carried out to prove the significant ductility of ECC components as an alternative to the common RC components [16]. Patel et al. [17] investigated the axial behavior of the short ultra-high-strength concrete filled steel tube through nonlinear finite element analysis. A reasonable steel contribution ratio could ensure its ductility. The results also pointed out the difference in the design equations between using normal-strength concrete and using ultra-high strength concrete. These studies proved that the hybrid structures can be effective for achieving an optimal design considering the economic cost and structural performance.

For the further application of the ECC material, this paper proposes the hybrid normal strength concrete (NSC)-ECC column, aiming at optimizing the column performance and economic cost. By using an exterior ECC layer, the crack resistance and ultimate deformability can be significantly improved, which is a possible way to achieve damage resistance and rapid recovery of the column. Furthermore, the exterior ECC layer can provide circumferential confinement for the core concrete due to its tensile strength. This paper investigated the load-carrying mechanism of the hybrid NSC-ECC column under large compression. First, a polypropylene-ECC (PP-ECC) material is described, which can reduce the cost while maintaining similar tensile performance compared with the PVA-ECC. With the development of PP-ECC, the hybrid NSC-ECC column, which has an exterior PP-ECC layer and RC core.

Seven column specimens, including one benchmark RC column, three comparative ECC columns, and three hybrid NSC-ECC columns, were tested. The yielding and failure modes and strain–stress relationships were obtained. According to the results, the hybrid NSC-ECC column delivered the satisfactory deformability and load-carrying capacity compared with the pure RC column. In addition, the hybrid NSC-ECC column provides an evident economic benefit without visible deterioration in mechanical performance. Further evaluations of the confinement effect and equivalent volumetric stirrup ratio were conducted. Finally, some design suggestions for the novel hybrid NSC-ECC columns are made.

2. Material property

The PP-ECC ingredients are shown in Table 1. With the employment of PP fiber, the cost per cubic meter decreased by almost 50% compared with PVA-ECC or PE-ECC [18]. Three PP-ECC panels were designed for the tensile tests. These specimens are shown in Fig. 1. A quasi-static load was applied according to Mo Li et al. [19]. The loading frame had sufficient stiffness and an ultimate capacity of 10 kN. The loading rate was selected as 0.05 mm/min [20]. The four aluminum plates had adequate stiffness to ensure the uniform distribution of the tensile force on the panel specimens. Two linear variable differential transformers (LVDTs) were used to monitor the axial deformation. The tensile test results are shown in Fig. 2. The PP-ECC presented evident strain-hardening behavior after the initial cracking. As the tensile deformation increasing, multiple fine cracks were formed on the surface of the PP-ECC panel.

Fig. 2a presents the cracking pattern of the PP-ECC. Multiple fine cracks were formed, but no fractures or PP fiber pull-out can be observed, even though the crack width was up to 4 mm. The strain–stress relationships are shown in Fig. 2b. The initial cracking stress f_{ti} was about 1.8 MPa. After initial cracking, the PP-ECC presented obvious strain hardening. The ultimate tensile strength f_{tu} was up to 3.3 MPa, corresponding to an ultimate tensile strain ε_{tu} of 0.05.

Compressive tests were conducted on a prism specimen measuring 100 × 100 × 300 mm. Table 2 summaries the mechanical properties of PP-ECC and C30 concrete. The tensile strength of C30 concrete was ignored in this study. Compared with the conventional C30 concrete, the PP-ECC delivered a smaller elastic modulus but similar compressive strength. The strain ε_{co} at the peak compressive stress was 0.0028 for PP-ECC and 0.002 for C30 concrete.

Table 1
Composition of PP-ECC.

Matrix /(kg/m^3)	Performance indicators of PP fibers				
Cement: 820 Polypropylene fiber: 18.2 Water: 504.8 Fly ash: 442	Volume ratio	Length (mm)	Density (kg/m^3)	Diameter (μm)	Stretch modulus (GPa)
	2%	12	0.91	20	5

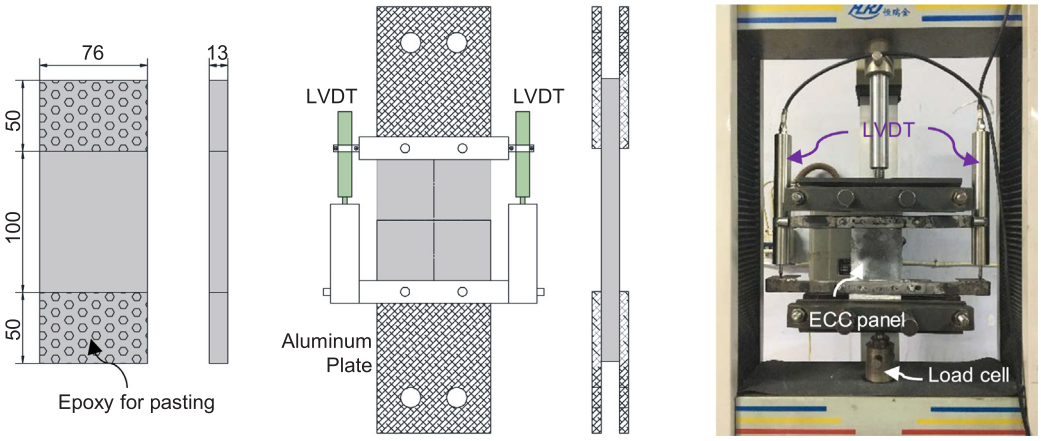

(a) Panel specimen (b) Loading and monitoring setup

Fig. 1. Tensile testing of PP-ECC.

3. Experimental program

3.1. Specimen design

The schematic of the specimens is shown in Fig. 3, including one conventional RC column, three PP-ECC columns, and three hybrid C30-PP-ECC columns. In the PP-ECC columns, the volumetric stirrup ratio was the main parameter. In the hybrid columns, there was an exterior PP-ECC layer around the internal RC column. Owing to the tensile strength of PP-ECC, the internal RC column could sustain stronger lateral confinement compared with a pure RC column. Moreover, the exterior PP-ECC layer can form multiple fine cracks during an earthquake, which is helpful for rapid recovery of its structural stability. In addition, the partial use of PP-ECC material in the hybrid columns has a lower cost than a pure PP-ECC columns.

All the specimens had the same diameter (d = 152 mm), height (h = 360 mm), and sectional reinforcement ratio (ρ = 1.1%). The upper and lower 60-mm segments were strengthened with stirrups to guarantee that yielding and damage would occur in the central segment. The rebar was HRB400 with a nominal yielding stress of 400 MPa. According to a tensile test, the yielding and ultimate stresses of the HRB400 rebar were 440 MPa and 610 MPa, respectively. Eight-mm rebar was used for the longitudinal reinforcement, and 6-mm rebar was used for the stirrups. The stirrup cover layer was 11 mm thick.

To investigate the axial behavior of the hybrid ECC column, in a total of seven specimens were designed, as shown in Table 3. One common RC specimen was designed as the benchmark specimen. Three reinforced PP-ECC columns were designed with different volumetric stirrup ratios, named as the E-series. The H-series was three hybrid C30-PP-ECC columns. The thickness of the exterior PP-ECC layer and volumetric stirrup ratio were the independent variables.

Table 2
Mechanical properties of PP-ECC and C30 concrete.

Material	E (MPa)	f_{ti} (MPa)	f_{tu} (MPa)	ε_{tu}	f_{co} (MPa)	ε_{co}
PP-ECC	12,800	1.8	3.3	0.05	29.04	0.0028
C30	24,800	–	–	–	30.02	0.002

The construction process of the hybrid column is shown in Fig. 4. Before the concrete and ECC material were poured, PVC sheets were arranged as the formwork and a reinforcement cage was placed in the formwork. First, the core C30 concrete was poured, and afterward the exterior ECC layer was poured. Before the initial setting, the interfacial formwork between the core C30 concrete and ECC layer was removed to ensure no separation of the interface between the two materials. Finally, after initial setting, the outer formwork was removed.

3.2. Loading and measurement system

The loading setup is shown in Fig. 5a. One displacement-controlled axial compression testing machine was used. The loading frame had a peak capacity of 100 tons. The loading speed was set as 0.5 mm/min, corresponding to a strain rate of 2.3×10^{-5}/s, which meets the requirements of Chinese concrete strength standards [19]. The measurement system is shown in Fig. 5b. An overall axial deformation was

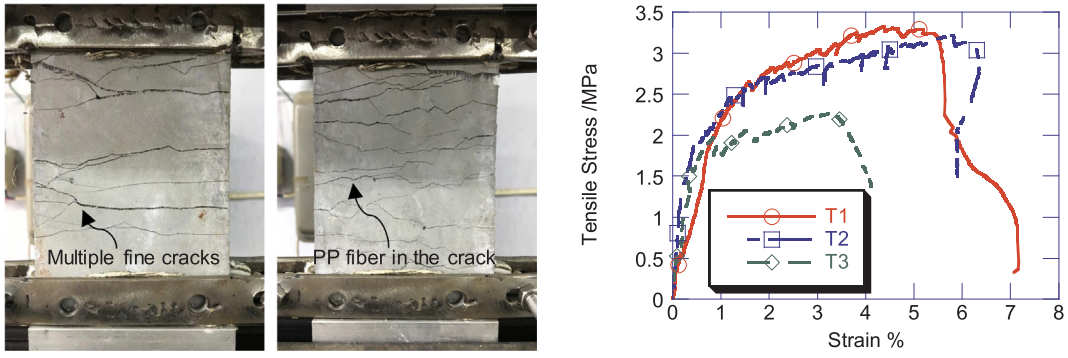

(a) Multiple fine cracks formed by loading (b) Strain–stress relationship

Fig. 2. Axial tensile testing of the PP-ECC panel.

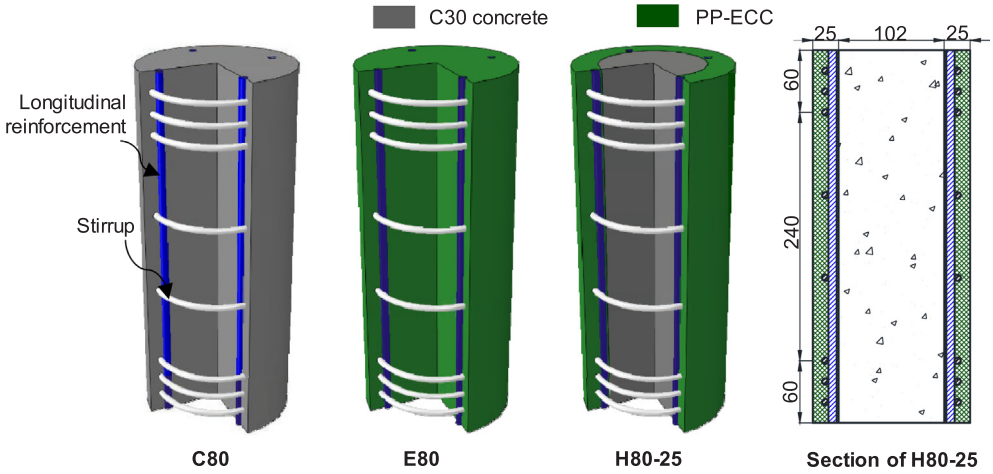

Fig. 3. Structures of the column specimens.

Table 3
Design parameters of specimens.

Specimen	Series	Volumetric stirrup ratio	Spacing of stirrup (mm)	Thickness of exterior PP-ECC layer (mm)
C80	Benchmark	1.6%	80	None
E80	ECC	1.6%	80	–
E120		1.06%	120	–
E00		0.0%	–	–
H80-10	Hybrid	1.6%	80	10
H80-25		1.6%	80	25
H120-35		1.06%	120	35

produced by the loading machine. A total of 16 strain gauges were pasted on the column along the vertical and lateral directions to measure the vertical compression and lateral expansion.

4. Experimental results

4.1. Failure mode

The failure modes of all the specimens are shown in Fig. 6. There were a few large cracks on the surface of the C80 specimen, which is a typical damage pattern for a C30 concrete cover layer under compression. In the confined ECC columns and NSC-ECC column, multiple fine cracking patterns can be observed instead of the localized large crack in the conventional concrete column. However, the ECC layer did not peel off, even after the stirrup fractured. The excellent tensile deformability of the PP-ECC could sustain an extremely large circumferential expansion. All the horizontal strain gauges were obviously subjected to tensile strains, that is, at least greater than 2×10^{-3} before failure. However, some strain gauges straddled the cracks and delivered very large strains, while other strain gauges provided much smaller strains. The randomly distributed vertical cracks led to inconsistencies in the monitored strain.

The maximum crack width was about 2 mm after the complete failure, and no fracture or PP fiber pull-out was observed. In contrast, the steel-fiber RC, that is, ultra-high-performance concrete and reactive powder concrete, usually release large amounts of energy suddenly due to steel fiber fracture and pull-out, resulting in obviously brittle failure [21,22]. In this regard, the PP fiber exhibited superior loading behavior by avoiding brittle failure.

As for the H-series, a vertical crack formed in the initial stage. Spalling of the 25-mm PP-ECC layer in H80-25 appeared just after the peak force was applied. Under larger compressive deformation, the C30 core collapsed first due to its inadequate deformability. Due to its dilatancy, damaged C30 concrete extruded through the surrounding PP-ECC layer. Because of the weak bonding strength at the C30/PP-ECC interface, the PP-ECC layer peeled off. Finally, H80-25 failed when the longitudinal reinforcement buckled. Similar failure modes were obtained in the other hybrid specimens.

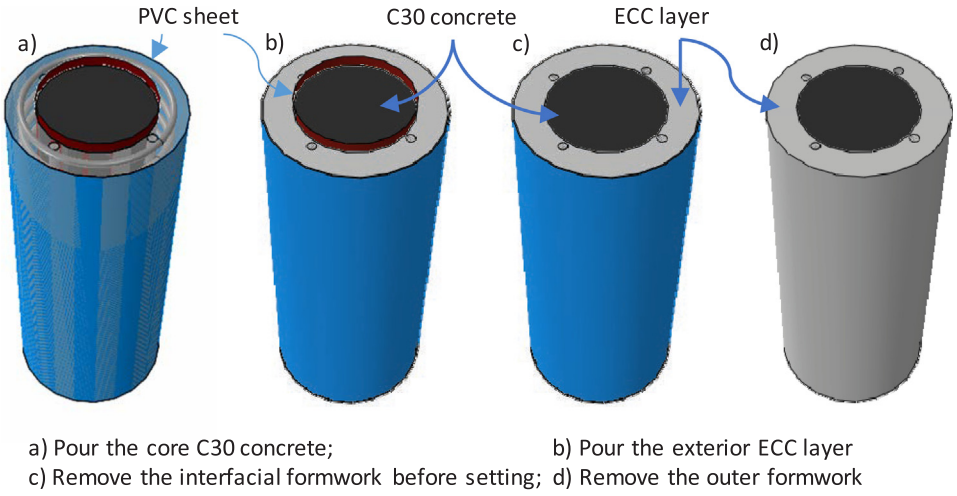

Fig. 4. Construction process of hybrid column.

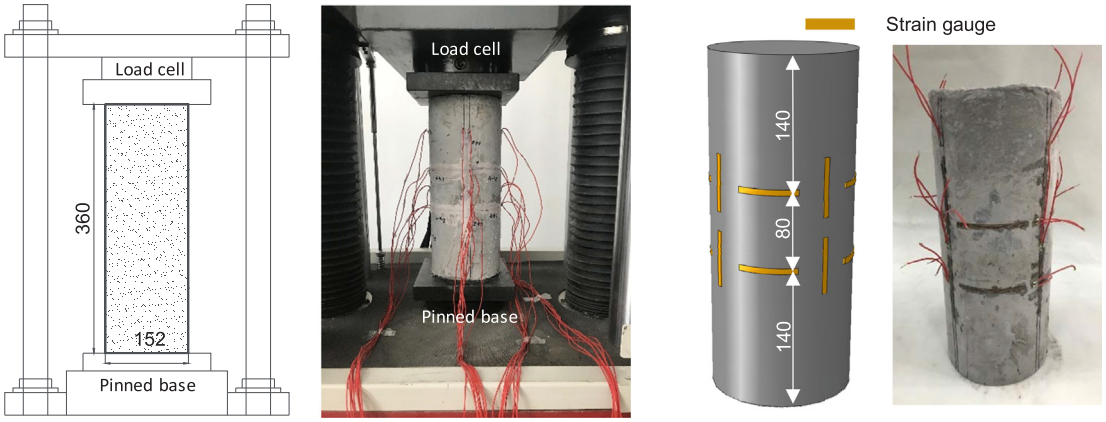

(a) Loading setup (b) Layout of strain gauges

Fig. 5. Loading setup and measurement system.

4.2. Axial strain–stress relationship

The axial strain–stress relationships are presented in Fig. 7. The confined stress was calculated as Eq. (1), where F, F_s, and F_{cov} are the overall axial load, axial load of the longitudinal reinforcement, and axial load of the cover layer, respectively; dc is the diameter of the center line of the stirrups; and ε is the axial compressive strain, calculated as overall deformation divided by total height (360 mm).

$$\sigma_c(\varepsilon) = \frac{F(\varepsilon) - F_s(\varepsilon) - F_{cov}(\varepsilon)}{\pi d_c^2/4} \tag{1}$$

$$F_s = \begin{cases} A_s E_s \varepsilon & \varepsilon \leqslant \varepsilon_y \\ A_s f_y & \varepsilon > \varepsilon_y \end{cases}, \quad F_{cov} = \begin{cases} A_{cov} E_c \varepsilon & \varepsilon \leqslant \varepsilon_{cov} \\ A_{cov} f_{co} & \varepsilon > \varepsilon_{cov} \end{cases} \tag{2}$$

Eq. (2) presents the method for calculating F_s and F_{cov}, where f_y and f_{co} are the yielding strength and axial compressive strength of rebar and ECC material, respectively, and E_s and E_c are the elastic moduli of the rebar and ECC material, respectively. According to Fig. 7a, the confined ECC column delivered higher peak strength and corresponding strain than the confined C30 concrete. The effect of the confinement was more evident in the ECC columns compared with that in the common C30 column. The main reason was the better deformability of ECC, which

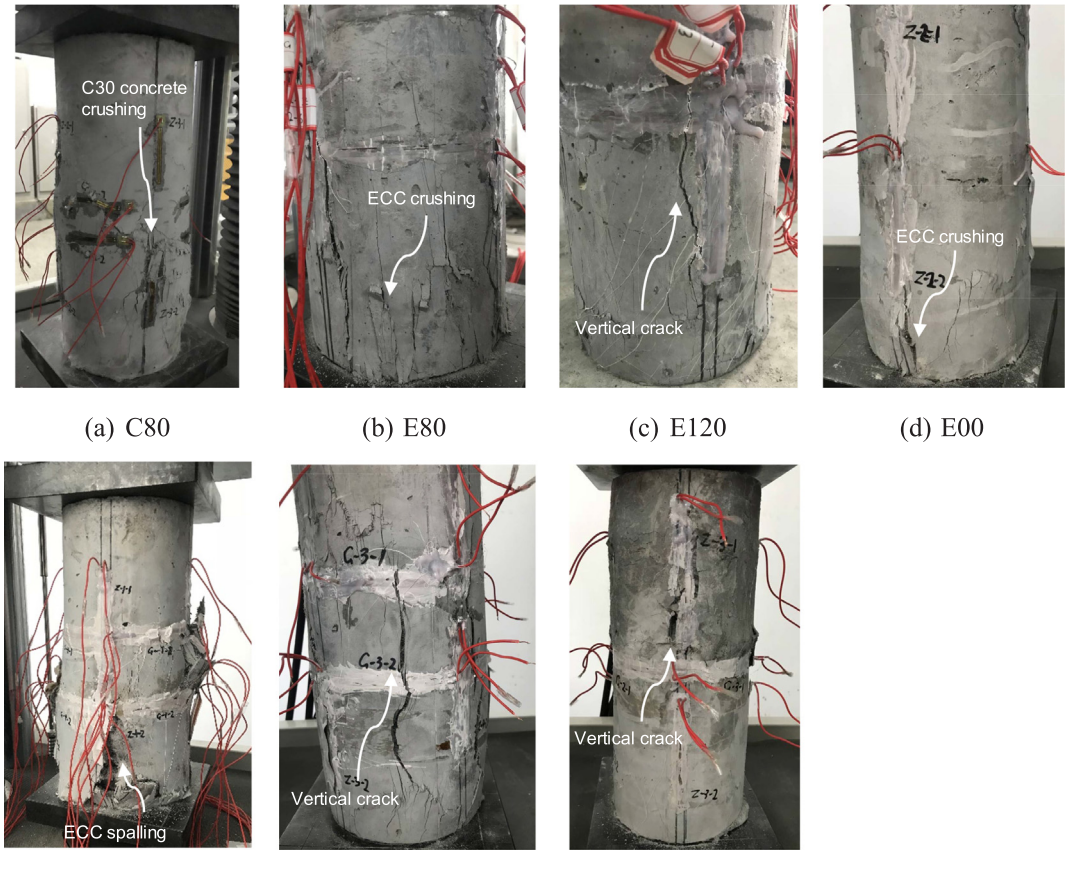

(a) C80 (b) E80 (c) E120 (d) E00

(e) H80-25 (f) H80-10 (g) H120-35

Fig. 6. Failure modes of test specimens.

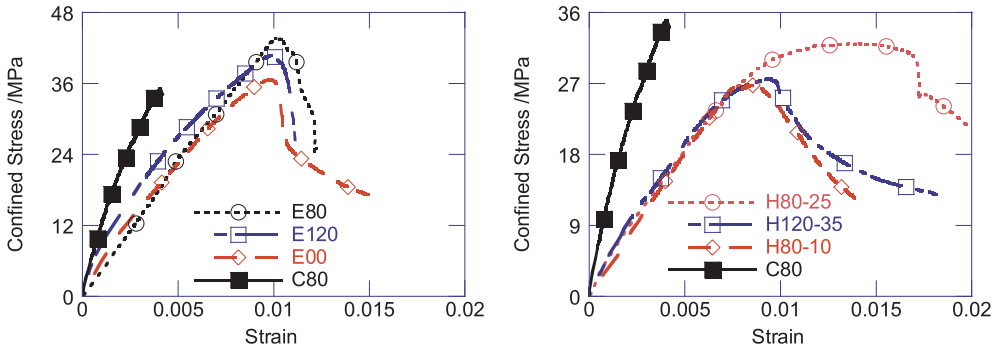

Fig. 7. Strain–stress relationship.

helped the stirrup provide more confinement force before the crushing occurred. Furthermore, the peak strength of the confined PP-ECC column increased with increasing volumetric stirrup ratio. Compared with the non-confined PP-ECC column E00, the peak compressive strengths of E80 and E120 presented 19.1% and 11.6% enhancements, respectively. In contrast, the strains at peak strength and the deterioration rate after peak strength were almost the same, regardless of the volumetric stirrup ratio. Under extremely large deformation, stirrups fractured. In addition, the circumferential expansion was too large to maintain the internal tensile capacity of PP-ECC, intensifying the loss of the confinement effect. The confined stress of the PP-ECC columns quickly decreased.

Fig. 7b shows the strain–stress relationships of the hybrid columns. The peak strengths of the hybrid columns were smaller than those of the PP-ECC columns, and even slightly smaller than that of C80. For example, H80-25 and H120-35 could provide 74% and 68% of the peak strengths of the corresponding PP-ECC columns with the same volumetric stirrup ratio. Owing to the different elastic moduli, the C30 core and PP-ECC layer could not achieve peak strength at the same deformation. The C30 core first achieved its peak strength, and the ECC layer contributed its peak strength later. Thus, there was a phase difference in the load-carrying capacities of the two materials. Thus, the overall strength of the hybrid column was smaller than that of the PP-ECC columns with the same volumetric stirrup ratio. Compared with the pure ECC material or C30 concrete, only H80-25 delivered enhanced strength, while H80-10 and H120-35 delivered less strength. To this end, the ECC layer must have adequate thickness when employed in practical applications. The comparison between H80-25 and H80-10 indicates that the thicker exterior PP-ECC layer could result in a larger overall strength and ductility. However, the tensile capacity of the exterior PP-ECC layer could not replace the confining effect of the stirrups according to the quicker deterioration of H120-35 with respect to H80-25.

Nevertheless, the hybrid columns delivered excellent deformability, which was much larger than that of C80. H80-25 retained the peak load-carrying capacity until the compressive strain reached 0.017, even larger than that of E80. The phase difference between the respective load-carrying capacities resulted in superior ductility. In H80-25, the load-carrying capacity was mainly provided by the C30 core in the initial stage due to its larger elastic modulus. When the load-carrying capacity of the C30 core was at its peak value, the PP-ECC layer provided a peak strength of only approximately 68%, according to the material test. After the peak strength of the C30 core was reached, the PP-ECC could further increase the load-carrying capacity and provide additional confinement for the C30 core. Thus, the overall load-carrying capacity did not decrease as quickly as a confined C30 column with the same volumetric stirrup ratio, and further overall increase may occur if a very thick PP-ECC layer is employed. In contrast, compared with the PP-ECC columns, the circumferential expansion of the C30 core was smaller than that of PP-ECC layer, indicating that the exterior PP-ECC layer could sustain larger axial compressive deformation.

5. Discussion

5.1. Confining effect of PP-ECC column

Fig. 8 compares the strain–stress relationship of the confined PP-ECC columns with the predictions from Mander [23] and Saatciglu [24]. The Saatciglu model could satisfactorily predict the peak confined strength and corresponded strain of the PP-ECC columns. The Mander model usually underestimated the confined strength and deformability of the PP-ECC. Furthermore, owing to the small elastic modulus of PP-ECC, the parabolic curves could not well trace the ascending segment of the strain–stress curves of the confined PP-ECC columns. Before the

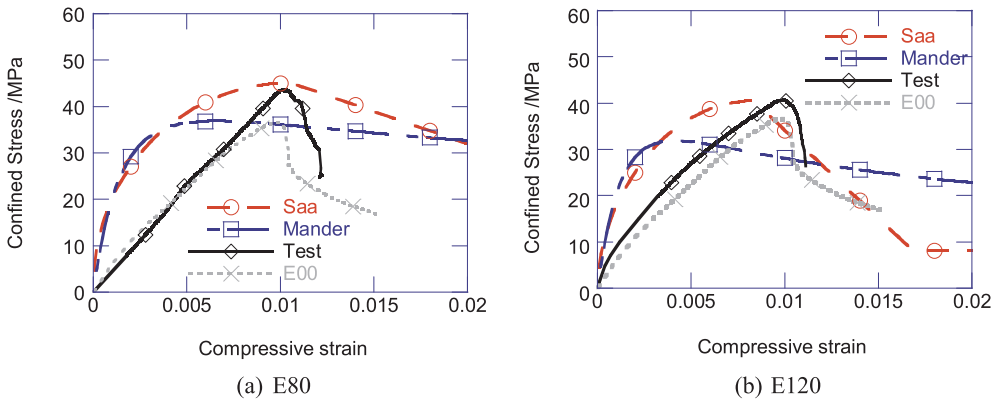

Fig. 8. Comparison of classic confined concrete models with test results.

peak strength, the strain–stress relationship of PP-ECC columns exhibited a slight linearity.

Deng et al. [25] developed an equation to estimate the concrete stress σ_{cc} in fiber-reinforced concrete, which is also applicable to the confined ECC columns. By assuming an isotropic elastic material, the confining stress can be derived as Eq. (3), where μ is Poisson's ratio ($\approx$0.2 for PP-ECC).

$$\sigma_{cc} = \sigma_{co} + \frac{1-\mu}{\mu}\sigma_l \tag{3}$$

In Eq. (3), σ_l is the circumferential confining stress in PP-ECC column, calculated by Eq. (4), where ρ_v is the volumetric stirrup ratio and σ_t is the tensile stress of PP-ECC. Eq. (4) was derived from reinforcement-confined ultra-high-performance concrete, and it delivered reliable predictions of the peak confined strength [25]. Eq. (4) only considers the confinement from the stirrup, and the contribution from the longitudinal reinforcement is ignored.

$$\sigma_l = \left(\frac{\rho_v E_s}{2E_{c\_ECC}} + 1\right)\sigma_t \tag{4}$$

The first component in Eq. (4) is the confining effect contributed from the stirrup and the second component comes from the tensile capacity of the fiber reinforced concrete. When σ_t reached the ultimate tensile strength f_t of PP-ECC, the compressive stress also reached its peak value. Table 4 compares the peak strengths suggested by Eq. (4) and the test result. The maximum relative error was less than 5%, demonstrating the effectiveness of Eq. (4).

In Fig. 7, replacing the inner PP-ECC core with the stiffer C30 concrete led to a decrease in the overall stiffness. According to Eqs. (3) and (4), the confining stress was important for the overall compressive stress. However, the C30 core of the hybrid column could not provide a self-confining stress because of its poor tensile capacity. According to the material property, the external confining stress contributed only about 12.4% of the overall confinement effect in E80, while is contributed 8.2% in E120. Thus, the overall confining stress in the hybrid columns was much smaller than that in the pure PP-ECC columns, leading to a decrease in the overall compressive stress. It can be concluded that the self-confining stress could evidently contribute to the overall stiffness of a confined PP-ECC column.

After the peak strength was reached, the deterioration rate of the PP-ECC was evidently faster than that from the predictions. According to the above strain analysis, the circumferential tensile strain achieved the ultimate tensile strain at the peak load. However, with a further increase in the circumferential tensile strain, the PP-ECC quickly lost its tensile capacity, that is, the self-confining effect deteriorated quickly. Considering the dominance of the self-confining effect in the confined PP-ECC columns, an overall rapid deterioration in the compressive capacity was observed

5.2. Load-carrying mechanism of hybrid column

The load-carrying mechanism is described in Fig. 9, which was abstracted from the test result of H80-25. The blue and red dashed curves indicate the contributions from the C30 core and exterior PP-ECC layer, respectively. The black solid curve indicates the total load-carrying capacity. In the initial stage, the load-carrying capacity of the C30 core and exterior PP-ECC both increased. Until reaching the strain $\varepsilon_{c\text{-}C30}$ at the peak strength of the C30 core, the contribution from the C30 core started to decrease. At this deformation, the contribution from the PP-ECC layer was still increasing. The overall behavior was controlled by the ratio of area between the C30 core and the exterior PP-ECC layer. However, the diameter of the C30 core, the thickness of the exterior PP-ECC layer, and the volumetric stirrup ratio also influenced the behavior of the confined C30 core. The overall behavior was not a simple sum of two independent parts. If the exterior PP-ECC layer was dominant, the overall load-carrying capacity continued to increase but with a small tangential stiffness. Otherwise, the load-carrying capacity decreased. Another noticeable deformation was the strain $\varepsilon_{c\text{-}ECC}$ at the peak strength of the exterior PP-ECC layer. Usually $\varepsilon_{c\text{-}ECC}$ is larger than the strain at the peak strength of pure PP-ECC, and even may be larger than the strain at the peak strength of reinforced PP-ECC. With more stirrups, the deformability of PP-ECC should be larger than that of the pure PP-ECC column. Compared with the reinforced PP-ECC column, the C30 core provided a small circumferential expansion to the exterior PP-ECC layer, which relieved the circumferential expansion trend. To this end, the exterior PP-ECC layer may sustain larger compressive deformation, even more than that of a reinforced PP-ECC column.

The analysis given above suggests that the actual peak force may occur at some deformation $\varepsilon_{c\text{-}H}$ between $\varepsilon_{c\text{-}C30}$ and $\varepsilon_{c\text{-}ECC}$. To describe the overall behavior of the hybrid column, three typical performance points can be noted: point A, the deformation at the peak strength of the C30 core; point B, the deformation at the global peak strength; and point C, the deformation at the peak strength of the exterior PP-ECC layer. Furthermore, at point B, the deterioration rate of the C30 core should equal the hardening rate of PP-ECC layer. The three typical performance points change dynamically according to the configuration of the hybrid columns, especially for the dimension ratio between the exterior PP-ECC layer and C30 core.

6. Conclusions

This study investigated the axial behavior of reinforcement-confined ECC columns and NSC-ECC hybrid columns. The confined PP-ECC and hybrid columns exhibited satisfactory ductility and confined strength. The confining effect in the ECC column was more evident than that in the conventional C30 column. The hybrid NSC-ECC column delivered excellent deformability. This study proves the potential for the application of ECC to the compression area of structures. Several conclusions are as follows:

(1) With the reinforcement confinement, the peak strength was improved by about 21%, but only 3.2% improvement was obtained in the ultimate deformability.
(2) The self-confining effect from the tensile capacity of ECC contributed almost 88% of the confining stress in specimen E80, which was important for the overall increasing stiffness, peak strength, and deterioration rate of the reinforced ECC column.
(3) The hybrid NSC-ECC column could deliver an excellent ultimate deformability, up to 0.017, while maintaining more than 95% of its peak strength.
(4) The overall performance of the hybrid column was dynamically affected by the ratio of the core C30 concrete to the exterior ECC layer. Further quantitative study of the hybrid column is needed.

Acknowledgments

This work was supported by the National Natural Science Foundation of China under grant No. 51708466, Sichuan Science and Technology Program under grant No. 2019YFH0139, the 17th key laboratory of Southwest Jiaotong University (open to undergraduate students) No. GD201817065, and the research plan of Shanghai Railway Bureau (2018145).

Table 4
Comparison of peak strength of steel-confined PP-ECC column.

	E80	E120
Test	43.66	40.72
Eq. (4)	43.04	42.55
Relative error	−1.43%	4.49%

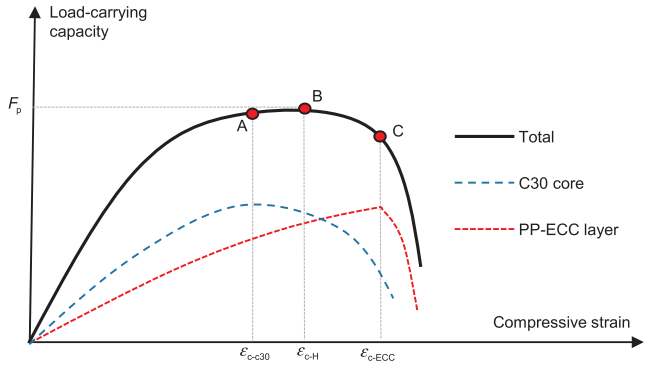

Fig. 9. Load-carrying mechanism of C30-PP-ECC hybrid column.

References

[1] Li VC, Wang S, Wu C. Tensile strain-hardening behavior of polyvinyl alcohol engineered cementitious composite (PVA-ECC) [J]. ACI Mater J-Am Concr Inst 2001;98(6):483–92.

[2] Yang X, Gao WY, Dai JG, et al. Flexural strengthening of RC beams with CFRP grid-reinforced ECC matrix [J]. Compos Struct 2018;189:9–26.

[3] Swolfs Y, Meerten Y, Hine P, et al. Introducing ductility in hybrid carbon fibre/self-reinforced composites through control of the damage mechanisms [J]. Compos Struct 2015;131:259–65.

[4] Said SH, Razak HA. The effect of synthetic polyethylene fiber on the strain hardening behavior of engineered cementitious composite (ECC) [J]. Mater Des 2015;86:447–57.

[5] Zhang R, Matsumoto K, Hirata T, et al. Application of PP-ECC in beam–column joint connections of rigid-framed railway bridges to reduce transverse reinforcements[J]. Eng Struct 2015;86:146–56.

[6] Tongfeng YJHYNZ, Ming L. Experimental research on mechanical properties of reinforced PP ECC beam [J]. Industrial Construction 2012:S1 [In Chinese].

[7] Said SH, Razak HA. Structural behavior of RC engineered cementitious composite (ECC) exterior beam–column joints under reversed cyclic loading [J]. Constr Build Mater 2016;107:226–34.

[8] Hung CC, El-Tawil S. Seismic behavior of a coupled wall system with HPFRC materials in critical regions [J]. J Struct Eng 2011;137(12):1499–507.

[9] Hossain KMA, Alam S, Anwar MS, et al. High performance composite slabs with profiled steel deck and engineered cementitious composite–strength and shear bond characteristics [J]. Constr Build Mater 2016;125:227–40.

[10] Choi WC, Yun HD, Cho CG, et al. Attempts to apply high performance fiber-reinforced cement composite (HPFRCC) to infrastructures in South Korea [J]. Compos Struct 2014;109:211–23.

[11] Maalej M, Leong KS. Engineered cementitious composites for effective FRP-strengthening of RC beams [J]. Compos Sci Technol 2005;65(7–8):1120–8.

[12] Maalej M, Lin VWJ, Nguyen MP, et al. Engineered cementitious composites for effective strengthening of unreinforced masonry walls [J]. Eng Struct 2010;32(8):2432–9.

[13] Hosseini F, Gencturk B, Lahpour S, et al. An experimental investigation of innovative bridge columns with engineered cementitious composites and Cu–Al–Mn super-elastic alloys [J]. Smart Mater Struct 2015;24(8):085029.

[14] Saiidi MS, O'Brien M, Sadrossadat-Zadeh M. Cyclic response of concrete bridge columns using superelastic nitinol and bendable concrete [J]. ACI Struct J 2009:106(1).

[15] Gencturk B, Elnashai AS. Numerical modeling and analysis of ECC structures[J]. Mater Struct 2013;46(4):663–82.

[16] Gencturk B, Elnashai AS, Lepech MD, et al. Behavior of concrete and ECC structures under simulated earthquake motion[J]. J Struct Eng 2012;139(3):389–99.

[17] Patel VI, Hassanein MF, Thai HT, et al. Ultra-high strength circular short CFST columns: axisymmetric analysis, behaviour and design [J]. Eng Struct 2019;179:268–83.

[18] Lin Zhan. Research on impact resistance of ECC crash barrier material. [D]. Doctoral Dissertation. Southeast University; 2017 [In Chinese].

[19] Li Mo, Victor C Li. Cracking and healing of engineered cementitious composites under chloride environment. ACI Mater J 2011;108(3):335–6.

[20] Ministry of Housing and Urban-Rural Construction of the People's Republic of China. Standard for evaluation of concrete compressive strength. China Construction Industry Publishing House; 2010 [In Chinese].

[21] Zhao C, Wang K, Zhou Q, et al. Full-scale test and simulation on flexural behavior of dovetail-shaped reactive powder-concrete wet joint in a composite deck system [J]. J Bridge Eng 2018;23(8):04018051.

[22] Yang X, Zohrevand P, Mirmiran A. Behavior of ultrahigh-performance concrete confined by steel [J]. J Mater Civ Eng 2016;28(10):04016113.

[23] Mander JB, Priestley MJN, Park R. Theoretical stress-strain model for confined concrete [J]. J Struct Eng 1988;114(8):1804–26.

[24] Saatcioglu M, Razvi SR. Strength and ductility of confined concrete [J]. J Struct Eng 1992;118(6):1590–607.

[25] Deng K, Xu R, Zhao C. Technical report of the axial compressive test on the reinforcement confined UHPC [R]. Southwest Jiaotong University; 2018.